

Diffusion-based subsurface multiphysics monitoring and forecasting

Xinquan Huang , Fu Wang , Tariq Alkhalifah
King Abdullah University of Science and Technology
{xinquan.huang,fu.wang,tariq.alkhalifah}@kaust.edu.sa

Abstract

Carbon capture and storage (CCS) plays a crucial role in mitigating greenhouse gas emissions, particularly from industrial outputs. Using seismic monitoring can aid in an accurate and robust monitoring system to ensure the effectiveness of CCS and mitigate associated risks. However, conventional seismic wave equation-based approaches are computationally demanding, which hinders real-time applications. In addition to efficiency, forecasting and uncertainty analysis are not easy to handle using such numerical-simulation-based approaches. To this end, we propose a novel subsurface multiphysics monitoring and forecasting framework utilizing video diffusion models. This approach can generate high-quality representations of CO₂ evolution and associated changes in subsurface elastic properties. With reconstruction guidance, forecasting and inversion can be achieved conditioned on historical frames and/or observational data. Meanwhile, due to the generative nature of the approach, we can quantify uncertainty in the prediction. Tests based on the Compass model show that the proposed method successfully captured the inherently complex physical phenomena associated with CO₂ monitoring, and it can predict and invert the subsurface elastic properties and CO₂ saturation with consistency in their evolution.

Key points

- We develop a novel monitoring and forecasting framework using video diffusion models of subsurface changes due to, for example, CO₂ injection.
- This video generation framework can be a simulation engine for multiphysics evolution, as well as maintain a physical consistency between different physical parameters, thus enabling subsequent forecasting and monitoring.
- The proposed framework is successfully applied to multiphysics monitoring and forecasting for permeability, CO₂ saturation, velocity, density, and reverse time migration (RTM) images.

1 Introduction

Carbon capture and storage (CCS) play a crucial role in mitigating greenhouse gas emissions, particularly from industrial outputs. This significance is underscored in the recent International Panel on Climate Change report [IPCC, 2022]. CCS involves capturing carbon dioxide (CO₂), transporting it, and injecting it into subsurface storage sites. However, to ensure its effectiveness and mitigate associated risks, monitoring, verification, and accounting of the injected CO₂ plume are essential [Sun et al., 2023]. Effective monitoring hinges on accurate and robust systems. Seismic monitoring, as highlighted by Lumley [2010], can provide such a system that is both accurate and covers a large area. It operates on the principle that CO₂ injection alters the elastic properties of the subsurface, such as velocities and densities. These changes can be inferred, to some extent, from the imaging and inversion of seismic recordings [Bosch et al., 2010, Hicks et al., 2016, Li and Alkhalifah, 2022, Hu et al., 2023]. However, conventional methods like statistical (e.g., Monte Carlo simulation) or wave equation-based approaches are computationally demanding and thus costly for realistic applications. In addition to the monitoring, predicting the future states of CO₂ flow is also important as they can provide information on how much CO₂ can be stored safely and help us optimize our decisions with

respect to injections. Using the above conventional methods, we struggle to track the CO₂ plume evolution and predict future subsurface states. Solving non-linear partial differential equations for a multi-phase flow phenomenon [Pruess and Nordbotten, 2011] can help us predict future states based on historical states, but this prediction is still computationally expensive [Witte et al., 2023].

In the era of artificial intelligence, modern machine-learning techniques have opened new avenues to tackle the above issues. Recent studies [Li et al., 2018, Zhong et al., 2019, Zhou et al., 2019, Li et al., 2020, Wen et al., 2021, 2022, Witte et al., 2023, Louboutin et al., 2023b, Yin et al., 2023b, Sun et al., 2023, Stepien et al., 2023, Gahlot et al., 2023] have leveraged machine learning techniques for various aspects of CCS monitoring and forecasting. Yet, these methods primarily focus on leakage detection, accelerating CO₂ plume simulation and the CCS modeling, single physics and 2D mapping with generative models, or cascade multiphysics inversion. Real-world monitoring and forecasting of subsurface CO₂ injections involve a complex multiphysics process encompassing fluid flow simulation, rock physics, and wave propagation.

To achieve an end-to-end multiphysics inversion and maintain the consistency of the evolution of different variables in terms of physical laws, we introduce a novel diffusion model-based framework for monitoring and forecasting in this paper. Instead of using 2D denoising diffusion probabilistic models (DDPMs) [Ho et al., 2020] to learn the inverse mapping between the seismic gather shots and the CO₂ plume shape [Sun et al., 2023], our framework trains a diffusion model to learn the data distribution of 3D multiphysics evolution (spanning 2D spatial and 1D time-lapse domains). This 3D volume incorporates variables such as permeability, CO₂ saturation, velocity, density, and reverse time migration (RTM) images. The philosophy behind the use of 3D volume (video) prediction is that the physical process in the real world can be regarded as video sequences. Thus, the forecasting and inversion process will be thought of as the tasks for video generation given the history frames or partial information. Unlike recursively predicting the future states along the time axis using a neural operator, which might have errors accumulation [Ding et al., 2024], the video diffusion model can simultaneously generate multistep future states. During inference, we employ reconstruction guidance to facilitate forecasting and inversion using historical frames or observed RTM images. Thanks to the probabilistic nature of the diffusion model, we can easily perform uncertainty analysis for forecasting and inversion. In this paper, we validate our method using the 3D Compass model [Jones et al., 2012].

The main contributions of this study include:

- We propose a monitoring and forecasting framework using video diffusion models.
- We show that the video generation framework can be a simulation engine for multiphysics evolution, as well as maintain a physical consistency between different physical parameters, thus enabling subsequent forecasting and monitoring.
- We validate the proposed framework on the compass model as we demonstrate the effectiveness of the proposed method in handling multiphysics monitoring and forecasting, specifically for permeability, CO₂ saturation, velocity, density, and reverse time migration (RTM) images.

The remainder of the paper is organized as follows. In section 2, we introduce the video diffusion models and the proposed framework for forecasting and monitoring based on video diffusion models with reconstruction guidance. Then, we share our numerical simulation for the data generation. In section 3, we present numerically test the proposed method on compass models, including the results of unconditional generation, monitoring, and forecasting. Finally, we discuss and summarize the work, and present insights in sections 4 and 5.

2 Methodology

Our proposed forecasting and inversion framework is based on video diffusion models. In this section, we begin with the definition of the forecasting and inversion frameworks as probabilistic predictions, which are smoothly connected to the denoising diffusion probabilistic models (DDPMs). After that, a detailed introduction about the key concepts and the pipeline behind the DDPMs as well as, the post-training controlled generation using reconstruction guidance will be provided. Finally, we introduce the variables describing the reservoir state used in this study to validate the effectiveness of the proposed method and related multiphysics processes.

2.1 Task definition

Both the forecasting and inversion can be formulated in a general form, in which, given the observations \mathbf{y} , which can be both the history states and current observation, we estimate multiple physical parameters \mathbf{x} (e.g., velocity or density change, CO₂ saturation) corresponding to current or future states. In a deterministic framework, it can be written as follows:

$$\mathbf{y} = f(\mathbf{x}), \quad (1)$$

where f denotes the modeling operator used for the inference of the future state given current/history states or for the inference of the current states as a response to observed data. However, for CO₂ monitoring and related multiphysics evolution, due to the complexity of subsurface behavior of CO₂ injection and related physical processes, geological uncertainties (such as those in our porosity and permeability measurements), technical limitations of the current observations, which may not be able to fully capture small leaks of carbon dioxide or complex geological changes, data analytics and the choice of assumptions and parameters in the modeling process introduce uncertainty. In other words, it is challenging to obtain accurate monitoring and forecasting results. Uncertainty is unavoidable.

Thus, we recast Equation 1 to a form in which we can draw samples from the conditional probability distribution, $p(\mathbf{x}^{1:T}|\mathbf{y})$, over T-steps monitoring or forecasting conditional on observations or previous/historical states \mathbf{y} . For a proof of concept, we form \mathbf{x}^t to represent 5 CO₂ related physical variables at time step t . To model $p(\mathbf{x}^{1:T}|\mathbf{y})$, instead of using ensemble methods with a learned neural network [Fort et al., 2020] or using the Bayesian method [Wilson and Izmailov, 2022], we use denoising diffusion probabilistic models (DDPMs) to model the distribution that allows us to draw samples from the distribution directly.

2.2 Video Diffusion models

Denoising diffusion probabilistic models (DDPMs) are a family of generative models that enable the generation of samples from a given distribution. They have shown a state-of-the-art image and video synthesis performance among other generative models, such as variational autoencoders [Kingma and Welling, 2013], generative adversarial networks [Goodfellow et al., 2014], normalizing flows [Rezende and Mohamed, 2015]. The general idea behind DDPMs is to train a neural network to learn to transform a prescribed distribution (often a Gaussian distribution) to an approximation of the target data distribution. The pipeline of the diffusion model includes two processes: training (a.k. forward process from \mathbf{x}_0 to \mathbf{x}_{T-1}) and sampling (a.k. reverse process from \mathbf{x}_{T-1} to \mathbf{x}_0), shown in Figure 1. The subscript T of the \mathbf{x}_T here denotes the time step in the diffusion process. Our target is to fit the data distribution of spatial-temporal evolution for multiple variables, which are 3D volumes. We process it as videos and thus use video diffusion models [Ho et al., 2022].

During the training, we corrupt the video with noise by gradually adding a small amount of Gaussian noise, and then train a neural network as a denoiser to restore the clean videos. For sampled data $\mathbf{x} \sim p(\mathbf{x})$, the corruption process (forward process) is a Gaussian process satisfying

$$q(\mathbf{x}_t | \mathbf{x}_{t-1}) = \mathcal{N}(\mathbf{x}_t; \sqrt{\alpha_t}\mathbf{x}_{t-1}, (1 - \alpha_t)\mathbf{I}), \quad q(\mathbf{x}_t | \mathbf{x}_0) = \mathcal{N}(\mathbf{x}_t; \sqrt{\bar{\alpha}_t}\mathbf{x}_0, (1 - \bar{\alpha}_t)\mathbf{I}), \quad (2)$$

where $q(\mathbf{x}_t | \mathbf{x}_{t-1})$ denotes transition distribution, \mathbf{x}_t denotes the corrupted videos at time-step t , where $0 \leq t \leq T-1$, $\alpha_t = 1 - \beta_t$, $\bar{\alpha}_t = \prod_{i=0}^t \alpha_i$, and β_t is the noise scheduler tasked with scaling the noise so that the corrupted videos at time T satisfy the Gaussian distribution $\mathcal{N}(0, \mathbf{I})$. We chose the cosine noise scheduler in this paper as it provides better performance and quality [Nichol and Dhariwal, 2021]. Similar to [Ho et al., 2020], instead of predicting the clean videos directly, the training process is realized by utilizing a neural network (3D Unet here) $\hat{\epsilon}_{\theta}(\mathbf{x}_t, t)$ to estimate the Gaussian noise ϵ for a given \mathbf{x}_t , and optimize the following loss function

$$\mathcal{L} = \mathbb{E}_{q(\mathbf{x}_t|\mathbf{x}_0)} \|\hat{\epsilon}_{\theta}(\mathbf{x}_t, t) - \epsilon\|^2, \quad (3)$$

where one can rewrite $\mathbf{x}_t = \sqrt{\bar{\alpha}_t}\mathbf{x}_0 + \sqrt{(1 - \bar{\alpha}_t)}\epsilon$.

At the stage of sampling (inference), we draw random samples \mathbf{x}_T from a Gaussian distribution and recursively denoise the videos by means of

$$\mathbf{x}_{t-1} = \frac{1}{\sqrt{\alpha_t}} \left(\mathbf{x}_t - \frac{1 - \alpha_t}{\sqrt{1 - \bar{\alpha}_t}} \hat{\epsilon}_{\theta}(\mathbf{x}_t, t) \right) + \sigma_q(t)\mathbf{z} \quad (4)$$

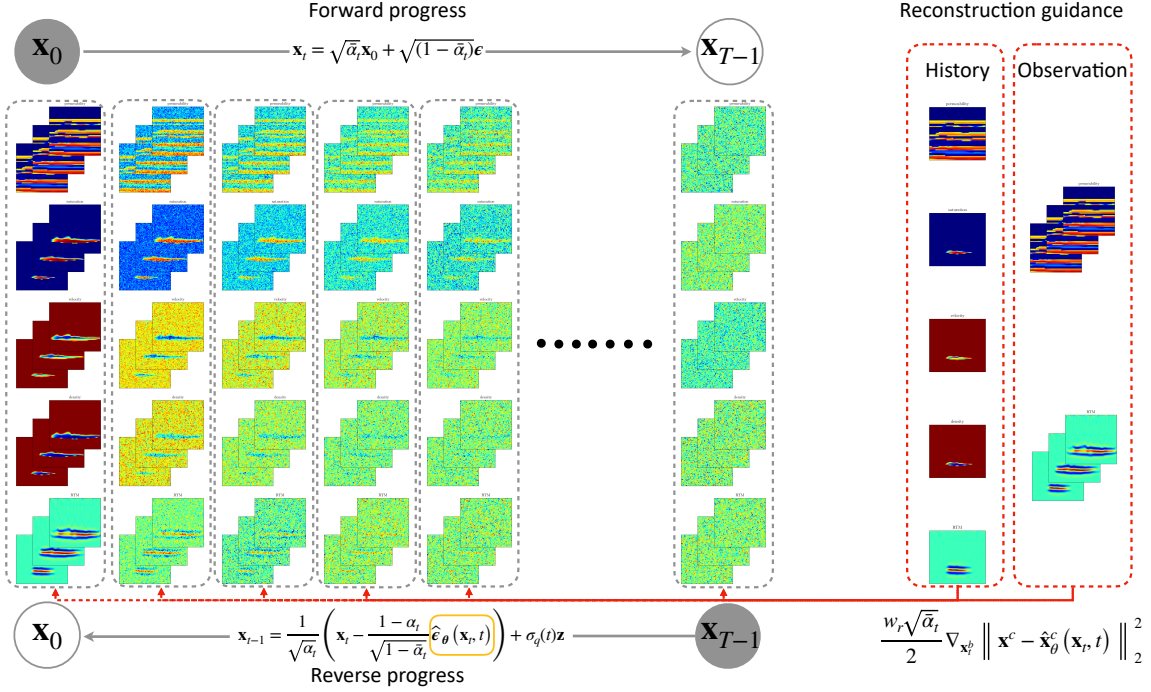


Figure 1: Workflow of the diffusion process and its reverse process, and the reconstruction guided generation for forecasting and inversion. The yellow box denotes the scaled learned score function.

until the final clean samples \mathbf{x}_0 are realized, where variance $\sigma_q(t) = \sqrt{\frac{(1 - \alpha_t)(1 - \bar{\alpha}_{t-1})}{1 - \bar{\alpha}_t}}$, \mathbf{z} is the standard Gaussian noise.

2.3 Reconstruction guided Conditional generation

As mentioned in section 2.1, our goal is to draw samples from the conditional probability distribution, which is stored in the video diffusion model, conditioned by the observations to achieve forecasting, inversion, and probabilistic prediction. Hence, to build $p(\mathbf{x}|\mathbf{y})$, the typical way is to directly incorporate the conditions in the neural network $\hat{\epsilon}_{\theta}(\mathbf{x}_t, t)$ as an additional input to replace the neural network prediction in equation 4. This would implicitly modify the sampling trajectory in the diffusion process to correct the samples to not only satisfy the stored distribution of the data themselves, but also be consistent with the conditions [Ho and Salimans, 2021]. However, this would require the retraining of the original unconditional diffusion model with sufficient data-label pairs to improve the generalization. In addition, for multi-physics monitoring and forecasting promoted here, the conditions in our framework are the history/current states of multiple variables or those obtained from imaging current surface observations using, for example, reverse time migration (RTM), where such images can be represented as \mathbf{x}^c . The superscript **c** here denotes the indexes of the frames and the variables. Here, \mathbf{x}^c denotes the given history frames (e.g., the history monitoring results, including velocity and density changes, permeability, saturation, and RTM images) as well as the observed frames (e.g., current seismic observations) or variables (e.g., constant permeability). That means the number of frames and the number of variables used as conditions are not fixed, which will increase the amount of training data.

Thus, in real applications, given the history frames and measurements, and to achieve conditional sampling $\mathbf{x} \sim p_{\theta}(\mathbf{x} | \mathbf{x}^c)$, we use reconstruction guidance [Ho et al., 2022]. As opposed to incorporating the conditions directly in the training process, we utilize a previously trained unconditional diffusion model to sample data given \mathbf{x}_t at each diffusion step. We then estimate the residuals between the conditions \mathbf{x}^c and the sampled results at the indices of the history states and/or observations. This is done by minimizing the l_2 norm of the reconstruction loss:

$$\|\mathbf{x}^c - \hat{\mathbf{x}}_{\theta}^c(\mathbf{x}_t, t)\|_2^2. \quad (5)$$

This approach allows us to effectively leverage the unconditional model while aligning the generated data with the given conditions.

Then, we can calculate the gradient of this loss function with respect to the \mathbf{x}_b , $\nabla_{\mathbf{x}_t^b} \|\mathbf{x}^c - \hat{\mathbf{x}}_\theta^c(\mathbf{x}_t, t)\|_2^2$, to correct the sampling projection in each diffusion step, where the superscript \mathbf{b} denotes the indexes of the target prediction complement to \mathbf{c} . Note that, unlike the usual way of calculating the gradient with respect to \mathbf{x}_t^c or the whole sample \mathbf{x}_t at time step t , instead, the gradient here is with respect to \mathbf{x}_b . The reason behind this formulation is that we hope to use the guidance, which represents the prediction at the conditional indexes \mathbf{c} and should be consistent with the given conditions, to alter the sampling within the manifold of the unconditional region to the sampling within the manifold shifted by the guidance. Our conditional diffusion model with reconstruction guidance is displayed in Figure 1. Hence, the new sampling procedure of the reverse diffusion process is changed from the original $\hat{\mathbf{x}}_\theta(\mathbf{x}_t, t) = (\mathbf{x}_t - \sqrt{1 - \alpha_t} \hat{\epsilon}_\theta(\mathbf{x}_t, t)) / \sqrt{\alpha_t}$ to

$$\tilde{\mathbf{x}}_\theta^b(\mathbf{x}_t, t) \leftarrow \hat{\mathbf{x}}_\theta^b(\mathbf{x}_t, t) - \frac{w_r \sqrt{\alpha_t}}{2} \nabla_{\mathbf{x}_t^b} \|\mathbf{x}^c - \hat{\mathbf{x}}_\theta^c(\mathbf{x}_t, t)\|_2^2, \quad (6)$$

where the additional term is the correction from the reconstruction loss, w_r is the weighting factor to control the strength of the guidance, and $\sqrt{\alpha_t}$ is to control the guidance at different reverse diffusion steps. The predictions at the conditional indexes \mathbf{c} are replaced by the conditions. With this framework, for example, if the network is trained on a small subset of six frames for computational efficiency, given the three history frames \mathbf{x}_c , we can predict the next three frames.

Besides the feasibility of the forecasting and inversion, with the reconstruction guidance, we can theoretically extend the multiphysics evaluation to an arbitrary length by autoregressive conditional generation. That means we can take the prediction $\mathbf{x}^{\frac{T}{2}:T}$ as the history states and use them as the condition to forecast the $\mathbf{x}^{T:\frac{3T}{2}}$. Then, by iteratively achieving this prediction, we can extend the forecasting to the out-of-scope distributions.

2.4 Uncertainty analysis

As mentioned above, we utilize the diffusion model to capture the joint distribution of multiphysics evolution. Then, starting from a batch of random noise as priors, we can generate multiple samples/realizations guided by the same observations and history states. Specifically, with the reconstruction guidance, we can generate samples that are all almost consistent with the conditions but slight variations may exist in areas not constrained well by the observations. We can measure the mean and variance of the generated samples as an estimate of uncertainty. Thus, in this paper, we will also showcase the estimated uncertainty using the proposed method in Section 3.

2.5 CO2 related Multiphysics datasets generation

The training data, especially those that offer accurate evolution of the multiphysics properties during CO2 injection, define the success of diffusion models, as they store the data distribution. However, in this study, our aim is to test the concept, so we make some simplifications and assumptions in our preparation of the training data. Since our objective is to demonstrate and realize an end-to-end multiphysics inversion and prediction, we prepared our training datasets based on multiphysics forward modeling techniques, as detailed in Louboutin et al. [2023b], and applied these techniques on synthetic data corresponding to the Compass velocity models. The forward process encompasses several stages: fluid flow simulation, followed by rock physics modeling, seismic modeling, and finally, reverse time imaging. For more intricate details of each stage in the forward process, we refer readers to Yin [2022], Yin et al. [2023b]. Additionally, Figure 2 illustrates the workflow used to prepare the training datasets.

Fluid flow simulation. Before we can simulate fluid flow, we need to define the permeability K of the subsurface model. Here, as suggested by Yin et al. [2023b], we convert the wave speed of the compass model to log-permeability values to make up alternating high- and low-permeability layers in the reservoir with a seal on top. The porosity used here is a constant value of 0.25. Then, we place one injection well in the deeper part of the target domain and consider a constant injection rate for the experiment here. After the injection, we use a two-phase simulation to obtain the CO₂ saturation model in Figure 2 with softwares Jutul.jl [Møyner et al., 2023] and JutulDarcyRules.jl [Yin et al., 2023a].

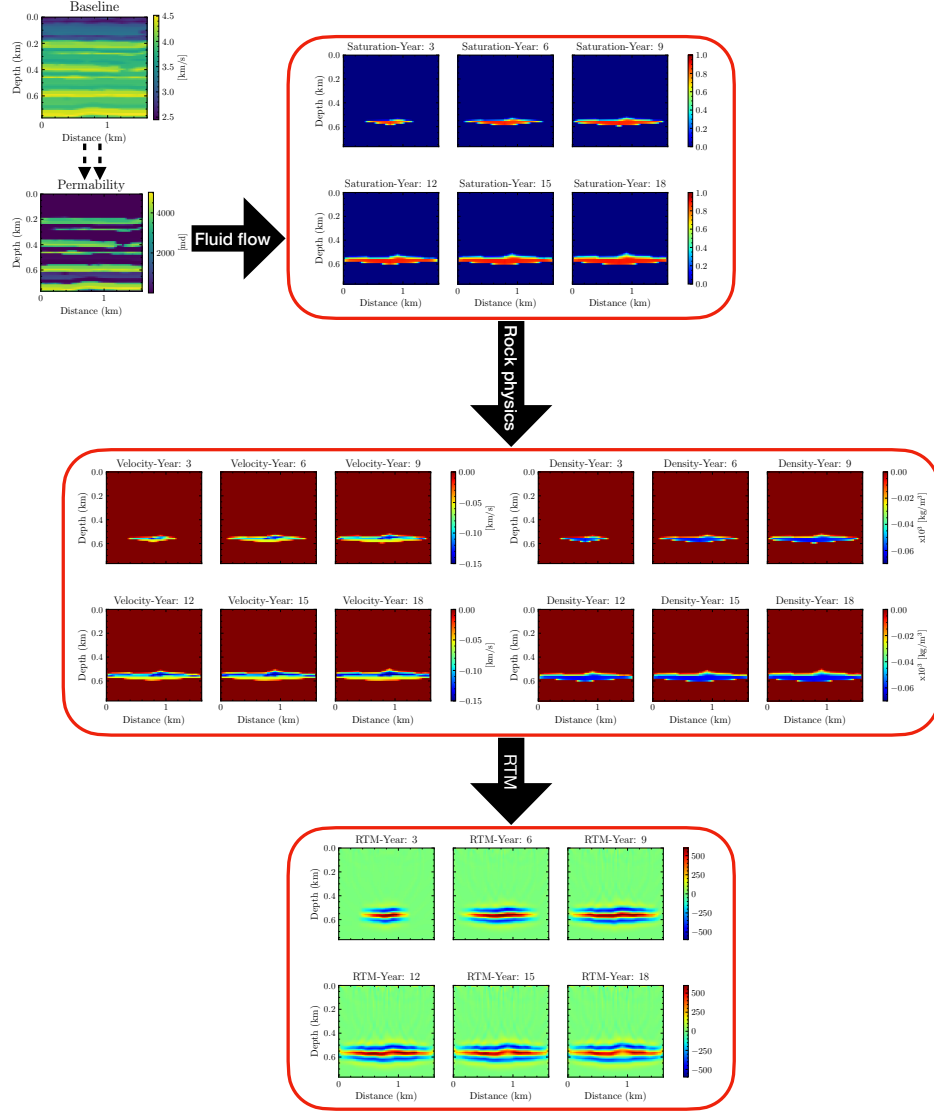


Figure 2: A multiphysics forward modeling framework starting with a permeability, which is converted from the baseline velocity model and then used to establish the CO₂ saturation given the constant injection using fluid flow simulation, which is in turn used to establish the changes in velocity and density based on rock physics modeling. Finally, the RTM images are obtained from the simulated data using the evolved velocity and density models.

Rock physics modeling. Since we use seismic methods to monitor the subsurface CO₂ changes, we need to obtain the velocity changes resulting from injection and the changes in saturation. We use the patchy saturation model [Louboutin et al., 2023b] to convert the saturation model to velocity and density models, in which an increase in CO₂ saturation will result in a decrease in velocity and density.

Seismic modeling and reverse time imaging. After obtaining the seismic properties changes provided by the velocity and density, we simulated the seismic response based on the impedance using born modeling and applied RTM to obtain images [Yin et al., 2023b] using the software JUDI.jl [Louboutin et al., 2023a]. The details on the source and receiver locations will be shared in the examples section. As the seismic responses to the velocity and density changes are quite small compared to the baseline monitoring, we do not use the RTM images directly. Instead, we use the residuals between the current RTM image and the baseline RTM image as the seismic observation. The Born modeling here will secure for us clean images as if processing and demultiple were applied to conventionally observed data.

2.6 The backbone network and training configuration

The backbone of the video diffusion model can have any architecture, e.g., 3D-Unet based [Cicek et al., 2016] or transformer based [Peebles and Xie, 2022]. In this paper, since we do not use a variational autoencoder to compress the videos to the latent space, using a transformer would be costly due to the quadratic computational complexity in the attention mechanism of the transformer. Thus, we use a 3D-Unet, which is factorized over space and time. Compared to the 2D Unet often used for image processing, whose convolutional layer is often with the kernel size of 3×3 , we use $1 \times 3 \times 3$ convolutional kernel for the video. The dimensions of the kernel correspond to the time frames, height, and width of the multiphysics evolution. The first attention block used in the 3D-Unet applies to the space dimension only, in which the time frame axis is regarded as the batch dimension, combined with a following temporal attention block. To distinguish the order of the frames (the time order of the multiphysics evolution), the relative position embeddings [Shaw et al., 2018] are used in each temporal attention block. This paper’s backbone network of the video diffusion model is designed to consider five channels, including permeability, CO₂ saturation, velocity, density, and RTM images.

The number of the timesteps T for the video diffusion is 1000, and the loss function of the training is given by the l_1 norm. To save on memory and stabilize the training, we use a gradient accumulation of 2, as well as mixed precision techniques [Micikevicius et al., 2018]. As has been used in many diffusion model training, we apply the Exponential Moving Average (EMA) [Xu et al., 2024] to smooth the parameters update of the neural network, improve the generalization, and accelerate the convergence.

3 Numerical Experiments

In our experiments, we employed the 3D Compass velocity model, a synthetic model that closely mimics the geological characteristics found in the southeastern region of the North Sea. This model serves as an ideal testbed due to its realistic representation of the subsurface geological features. We extract 800 two-dimensional slices from the three-dimensional compass velocity model, having dimensions of 64×64 , with an interval of 25 m in the horizontal direction and 12 m in the vertical direction. In this paper, we do not consider the leakage scenario and assume the permeability is constant over time, though this scenario can also be incorporated if needed. For the fluid flow simulation, we control the CO₂ injection rate to achieve a 10% storage capacity over an 18-year period. The constant CO₂ injection happens at the fixed well location (often known in field experiments). From this simulation, we sampled six frames starting from the third year with a time-lapse interval of three years. These frames were crucial in analyzing the temporal evolution of the injected CO₂. Subsequently, we applied rock physics modeling to calculate the corresponding changes in velocities and densities due to CO₂ injection for each CO₂ saturation at different times. We collected the simulated seismic data for each velocity and density model by placing six sources on the surface with a 24 Hz Ricker wavelet and 200 receivers on the sea bottom. The recordings lasted for 1 s with a sampling rate of 4 ms . Then, we employ RTM to compute the time-lapse seismic image changes by subtracting them from the baseline image. In the video diffusion training phase, we used an Adam optimizer with a learning rate of $1e-4$, a batch size of 64, and a maximum of 150,000 iterations until the neural network converged, as evidence by the training loss curve, shown in Figure 3.

3.1 Unconditional monitoring sampling

After completing the training of our diffusion model, we conducted an initial test by sampling multiphysics evolution over time without any conditions. Inputting two random noise samples in the latent space of the Diffusion model, we use equation 4 to do the reverse sampling for 1000 time steps. The results of this process are illustrated in Figure 4. As expected, we can see that starting from random Gaussian noise, we are able to generate high-quality spatial-temporal series for multiphysics evolution. The series showcased clear and detailed progression and maintained consistency with the underlying physical laws. It demonstrates that the diffusion model has successfully captured the inherently complex physical phenomena associated with CO₂ monitoring.

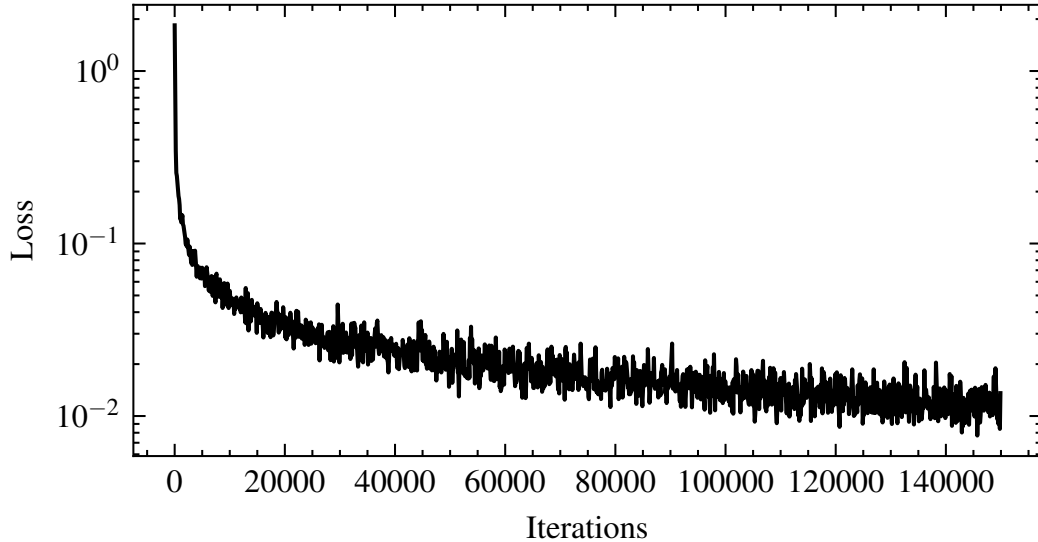


Figure 3: The training loss curve of the video diffusion model for multiphysics evolution.

3.2 Forecasting

As mentioned in Section 2, this well-trained unconditional video diffusion model can be used for forecasting and inversion. We first test it for the forecasting task to evaluate the ability to predict future CO_2 evolution based on the history frames as that can help us evaluate the capacity for CO_2 storage for decision-making optimization. With a reconstruction scale w_r of 1.0, the conditional sampling results are shown in Figure 5. Given the observations and records of the subsurface states in years 3, 6, 9, we forecast the future states for years 12, 15, and 18. They are consistent and reasonable in their evolution and generally maintain the coupling relationship between the five physical parameters. To quantitate the forecasting errors for each variable, we compare them with the reference numerical simulations, shown in Figure 6. The errors are small and are focused mainly in the region of the CO_2 plume. This generally validates our model’s accuracy and highlights its potential as a powerful tool for strategic planning in CO_2 storage projects.

3.3 Inversion

In realistic monitoring scenarios, besides the historical information of the multiphysics evolution, we might also have some measurements of the seismic response on the surface, such as the seismic recordings, which can be converted to RTM images [Li and Li, 2021]. RTM images play a crucial role in these instances, acting as a strong conditioner that can constrain and guide the generation of CO_2 evolution and the corresponding changes in subsurface elastic properties. With our method, we can do an inversion of the subsurface velocity, density, and CO_2 saturation, given the observed seismic images. To evaluate the effectiveness of this approach on inversion, we conducted tests where the generation process was conditioned by both historical frames and observed RTM image results. The inverted results are shown in Figure 7. We observed that the diffusion models can invert high-quality subsurface parameters, and the evolution of the inverted velocity, density, and CO_2 saturation are reasonable and consistent. We also quantify the errors of the inverted results using the reference numerical simulations, shown in Figure 8. Compared to the reference results, our method showcases a good inversion performance in terms of accuracy, especially for the velocity and density models, which the images are more dependent on. This makes sense as the more conditions we have, like the RTM image results, which can provide strong constraints on velocity and density, the better the accuracy of the prediction of our method.

Another scenario of inversion is that we only have the information on permeability and observations like RTM images and try to estimate the CO_2 saturation and elastic parameters. The inverted results using our proposed method are shown in Figure 9, and the quantitative analysis of the errors is shown in Figure 10. Besides good reconstruction of velocity and density changes, we find that the evolution of

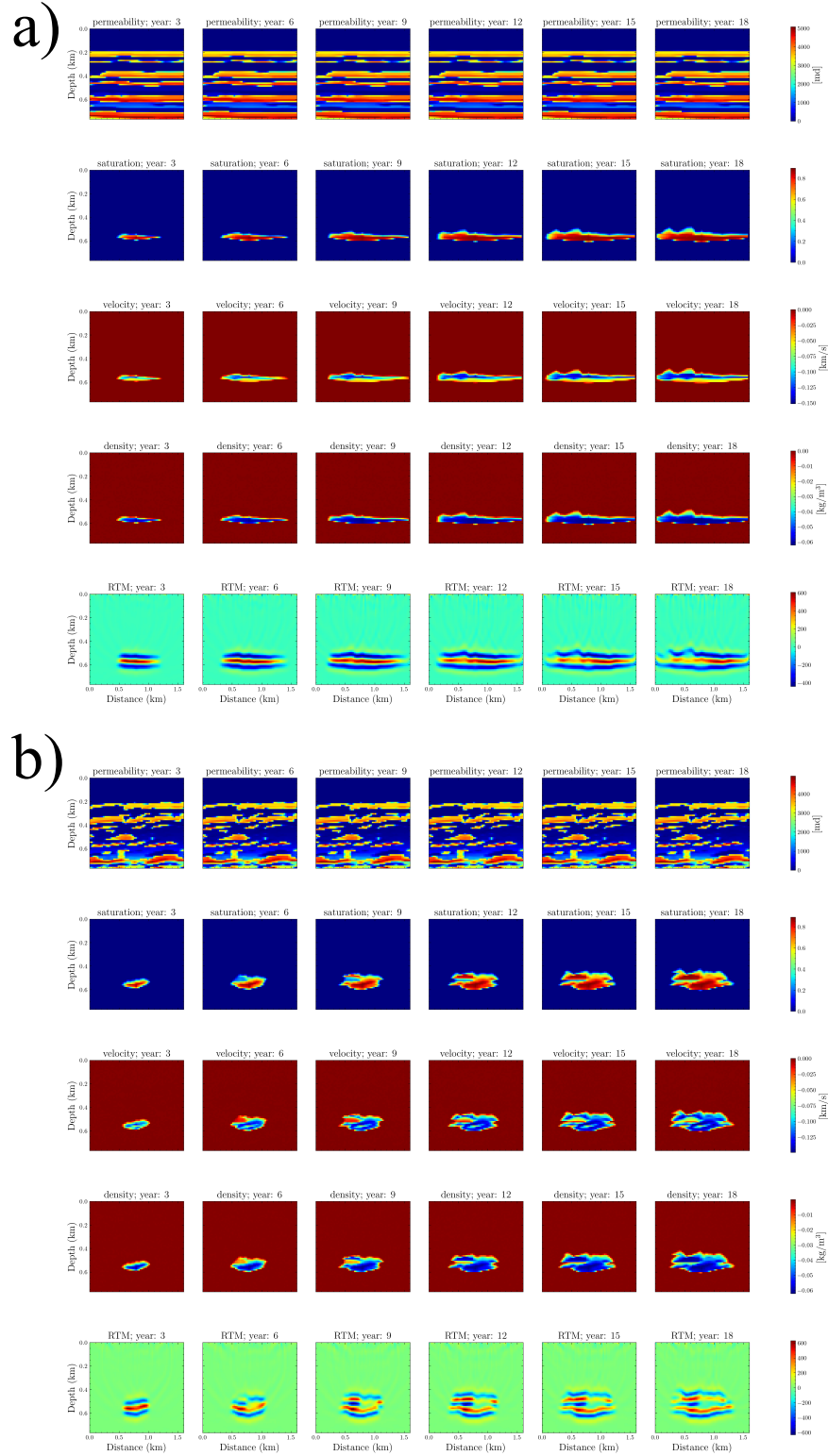


Figure 4: Uncoditional generation of multiphysics evaluation due to the CO_2 injection for two examples (a and b). Different frames denote different times with an interval of 3 years. Each row denotes a specific variable, including permeability, CO_2 saturation, velocity, density, and RTM images from top to bottom, respectively, while each column denotes the variables at different times.

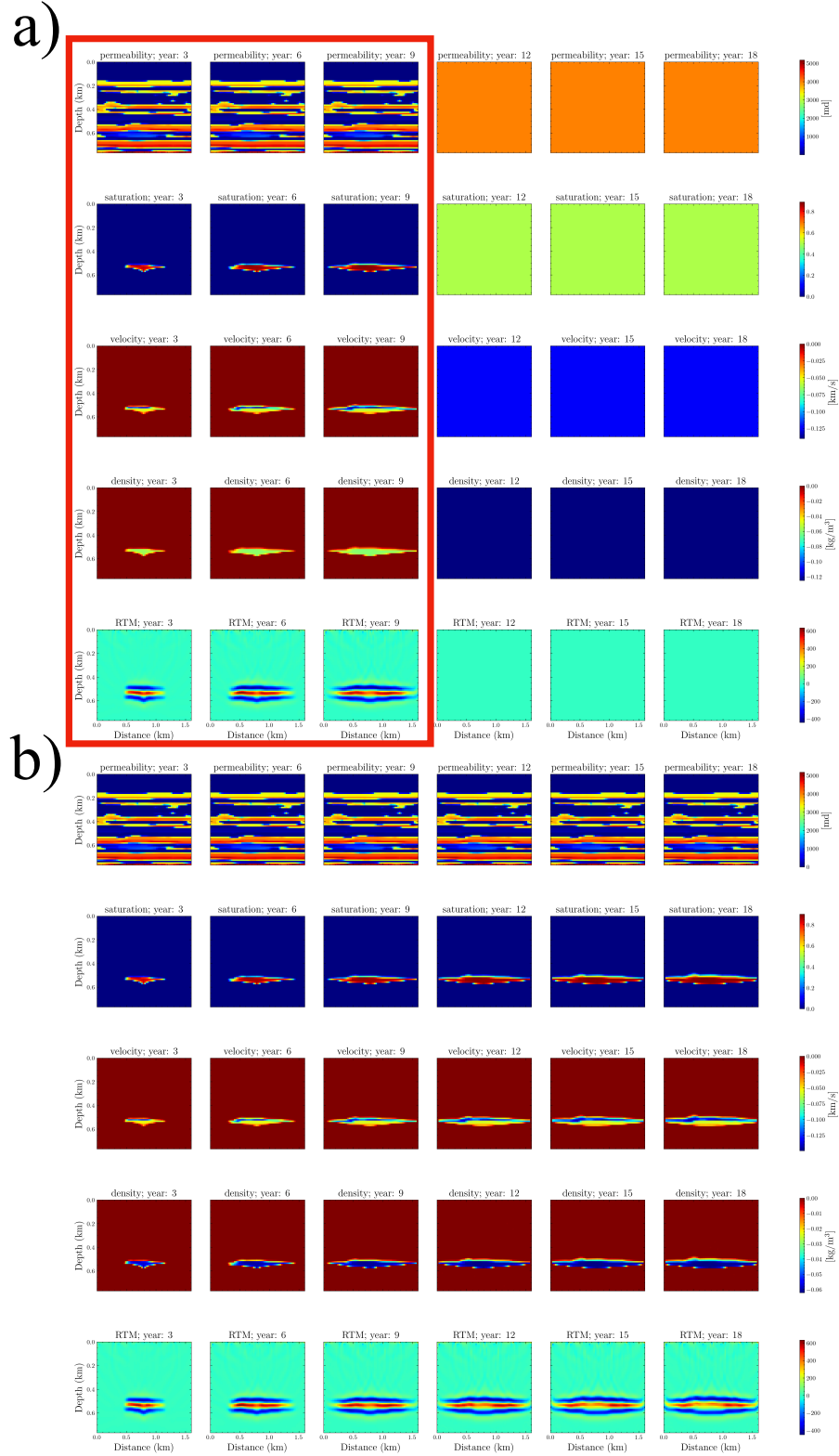


Figure 5: Forecasting generation (b) given three history frames (a), which are denoted by the red box. The rows represent properties described in Figure 4.

CO₂ is better estimated as we have accurate permeability information. This validates the importance of the permeability to the inference of CO₂ saturation.

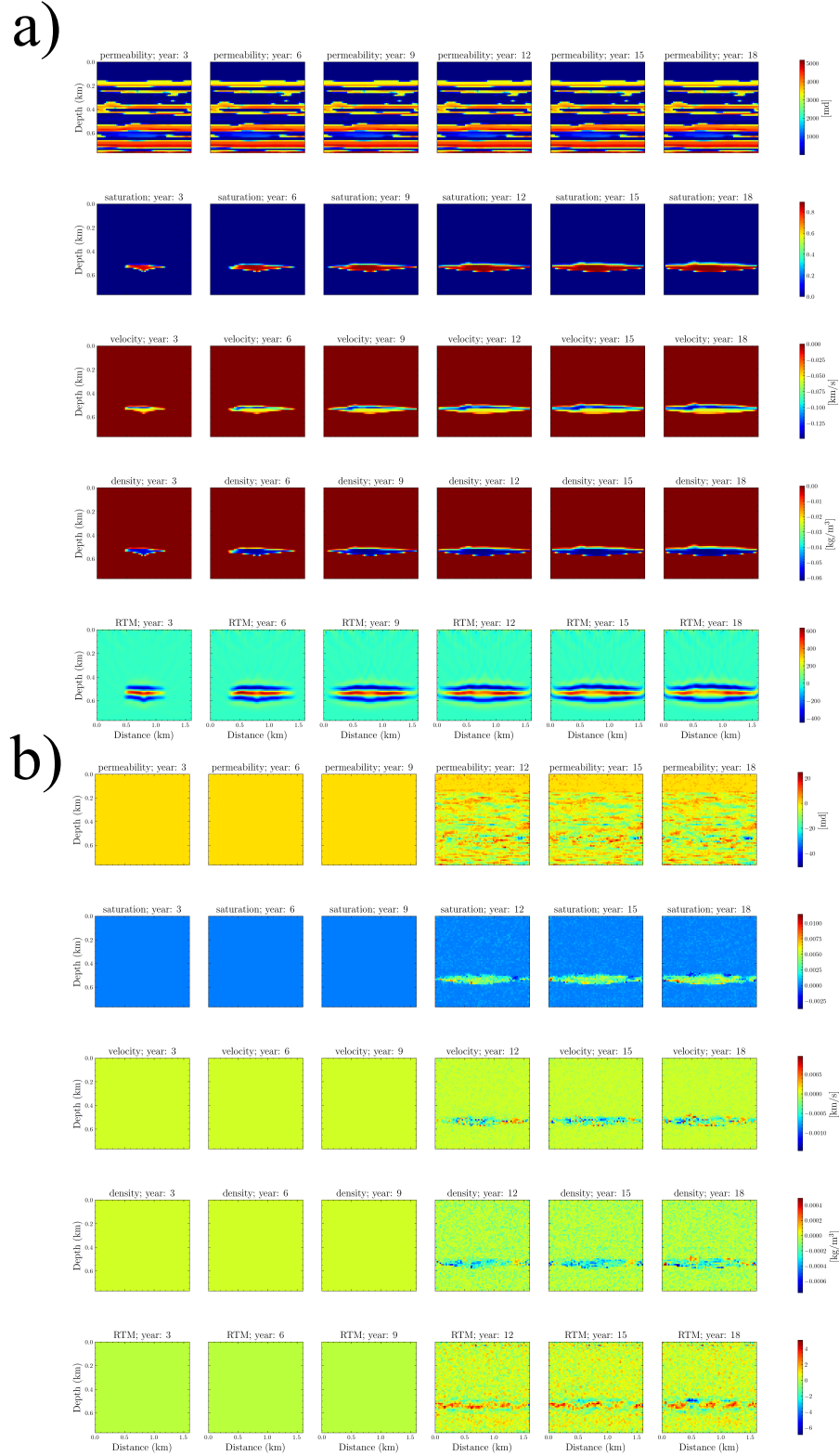


Figure 6: The errors (b) in forecasting generation (Figure 5b) compared to the reference (numerical) result (a). The rows represent properties described in Figure 4. The errors (differences) are plotted at the same scale.

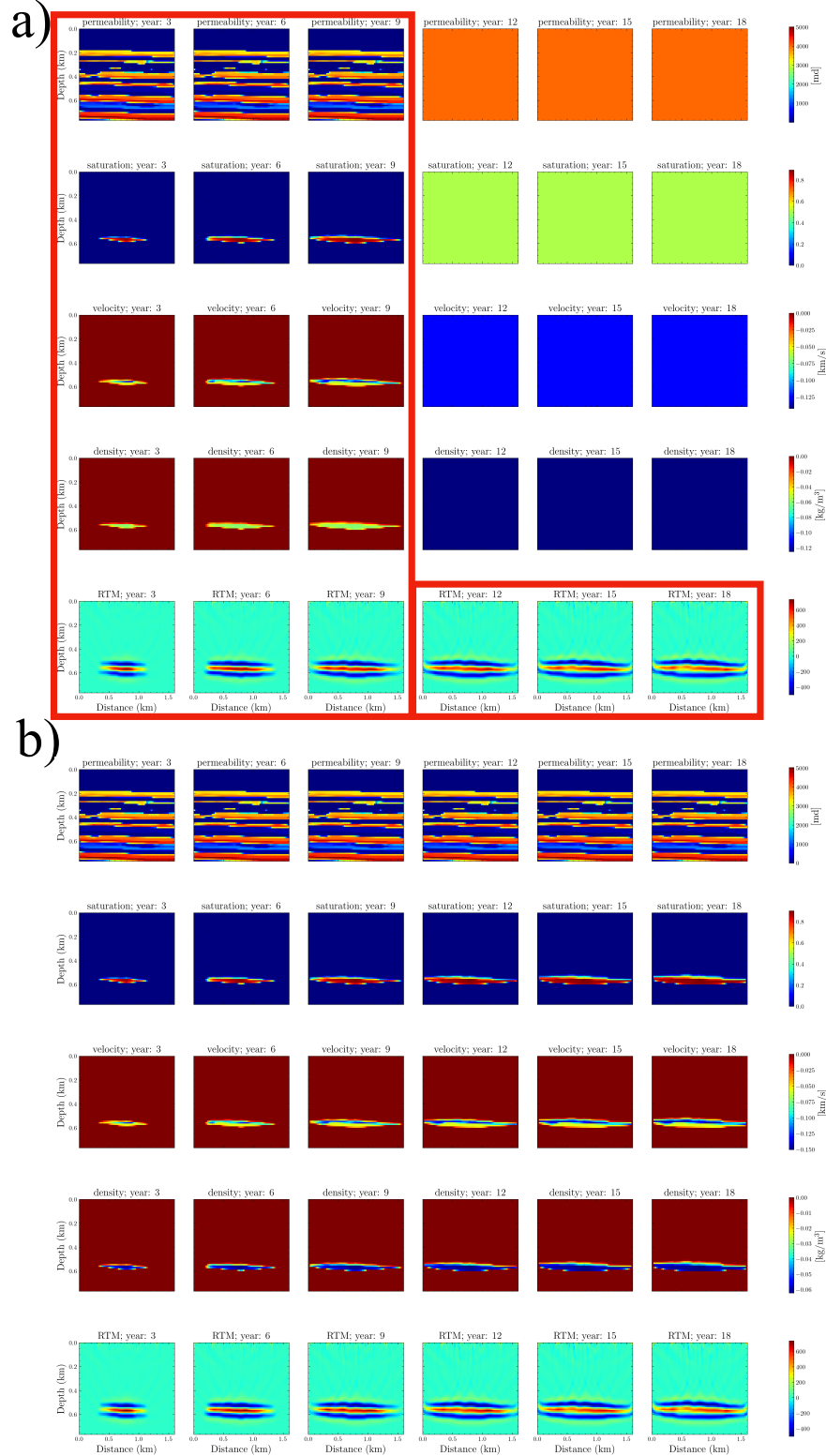


Figure 7: Inversion results (b) given three history frames and observed-data-based RTM images (a), which are denoted by the red box. The rows represent properties described in Figure 4

3.4 Out-of-scope forecasting

Combining the unconditional video diffusion model and reconstruction guidance, our framework can forecast not only the temporal scope of in-distribution but also the forecasting of the out-of-distribution

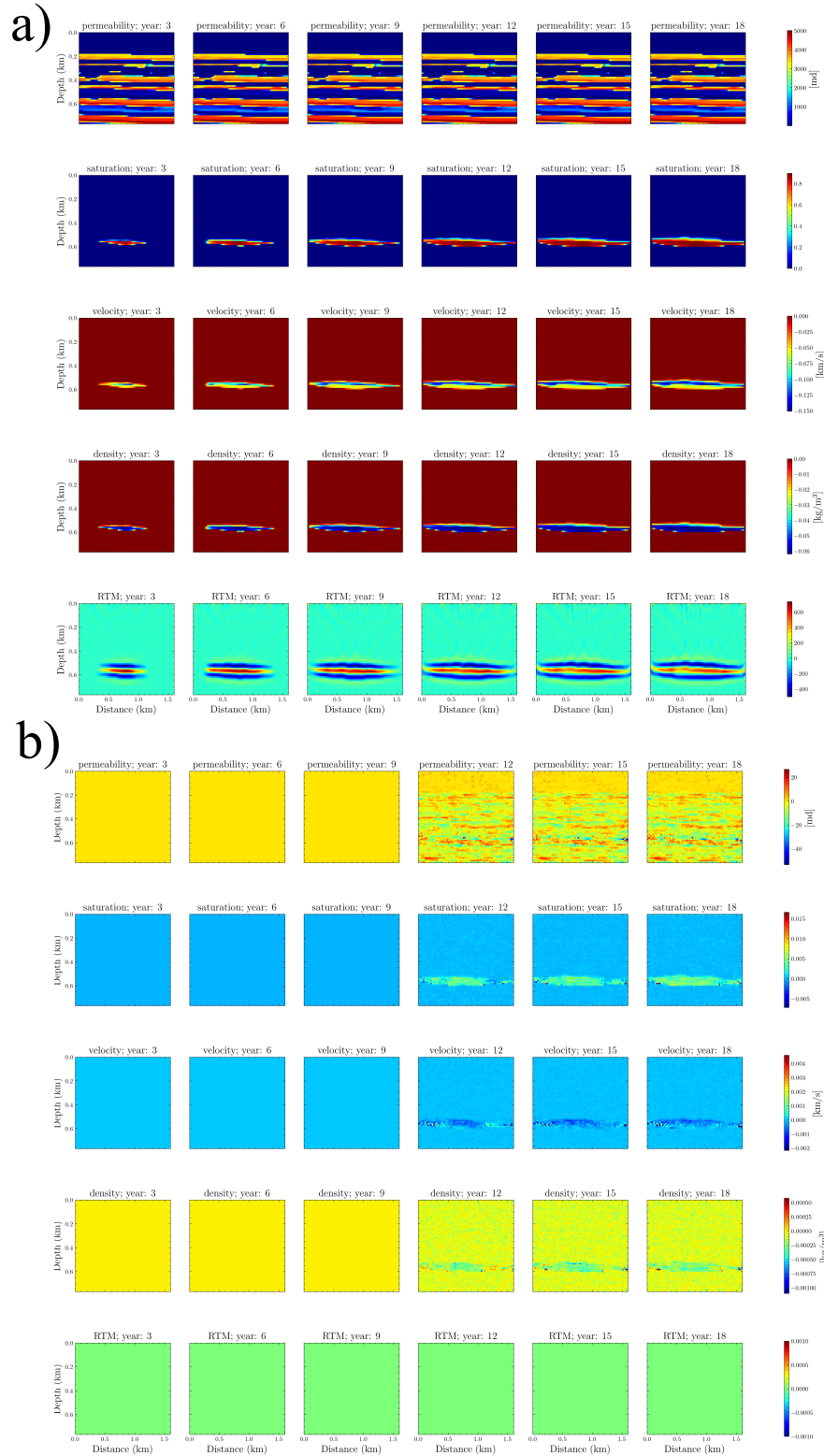


Figure 8: The errors (b) in the inverted results (Figure 7b) compared to the reference result (a). The rows represent properties described in Figure 4. The errors (differences) are plotted at the same scale.

scope by autoregressive conditional sampling. In theory, the proposed method can expand the evolution to arbitrary length. However, due to the limits of the spatial size of our simulation domain, the CO₂ plume at year 24 may exceed the boundary of the simulation domain, which is not the case in realistic

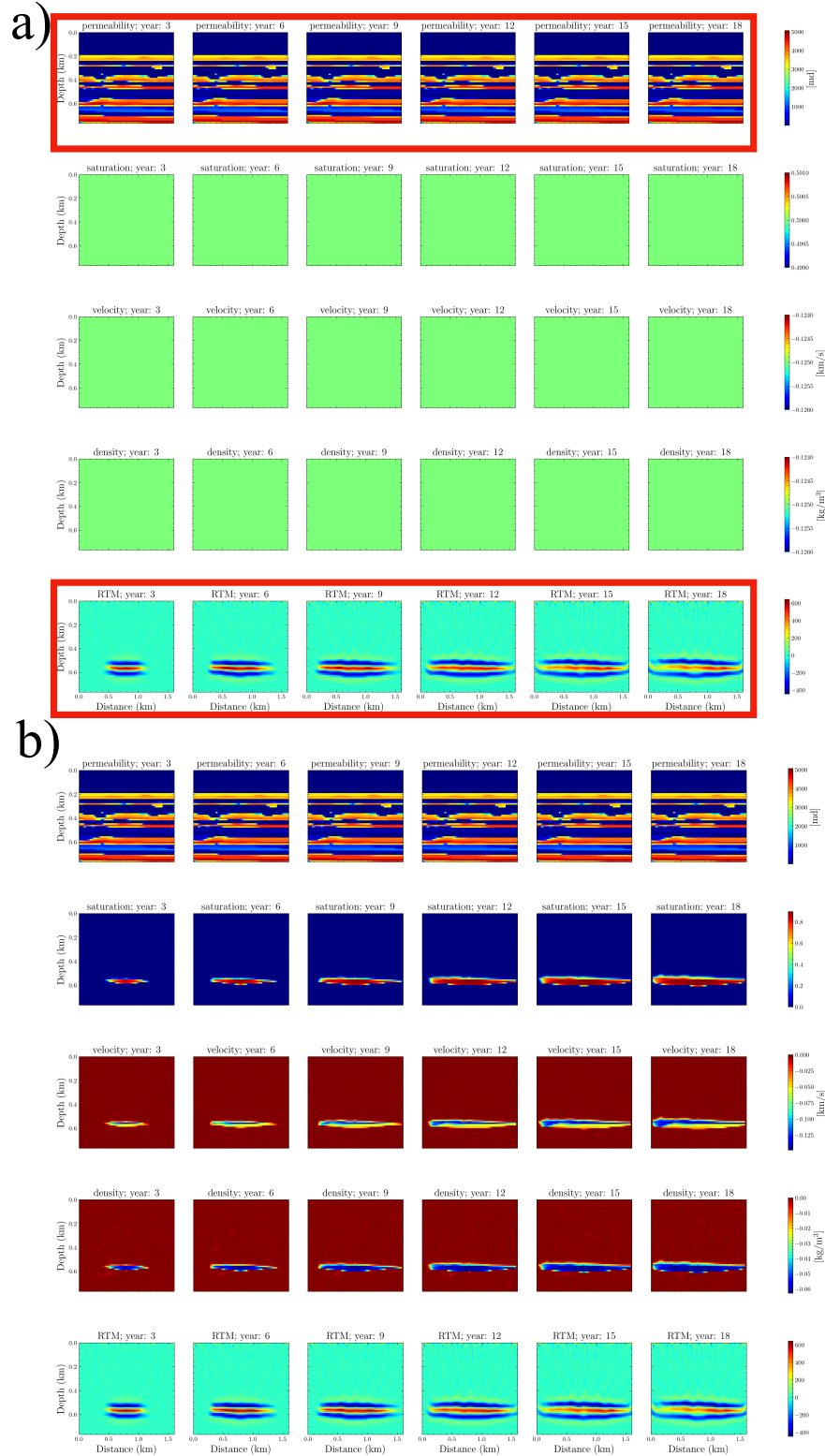


Figure 9: Inversion results (b) given permeability and observed-data-based RTM images (a), which are denoted by the red box. The rows represent the various monitored properties described in Figure 4

applications because our monitoring domain is usually bigger than the CO₂ plume. Hence, we first use the frames from 3, 6, and 9 years as history frames and the observations like RTM images and

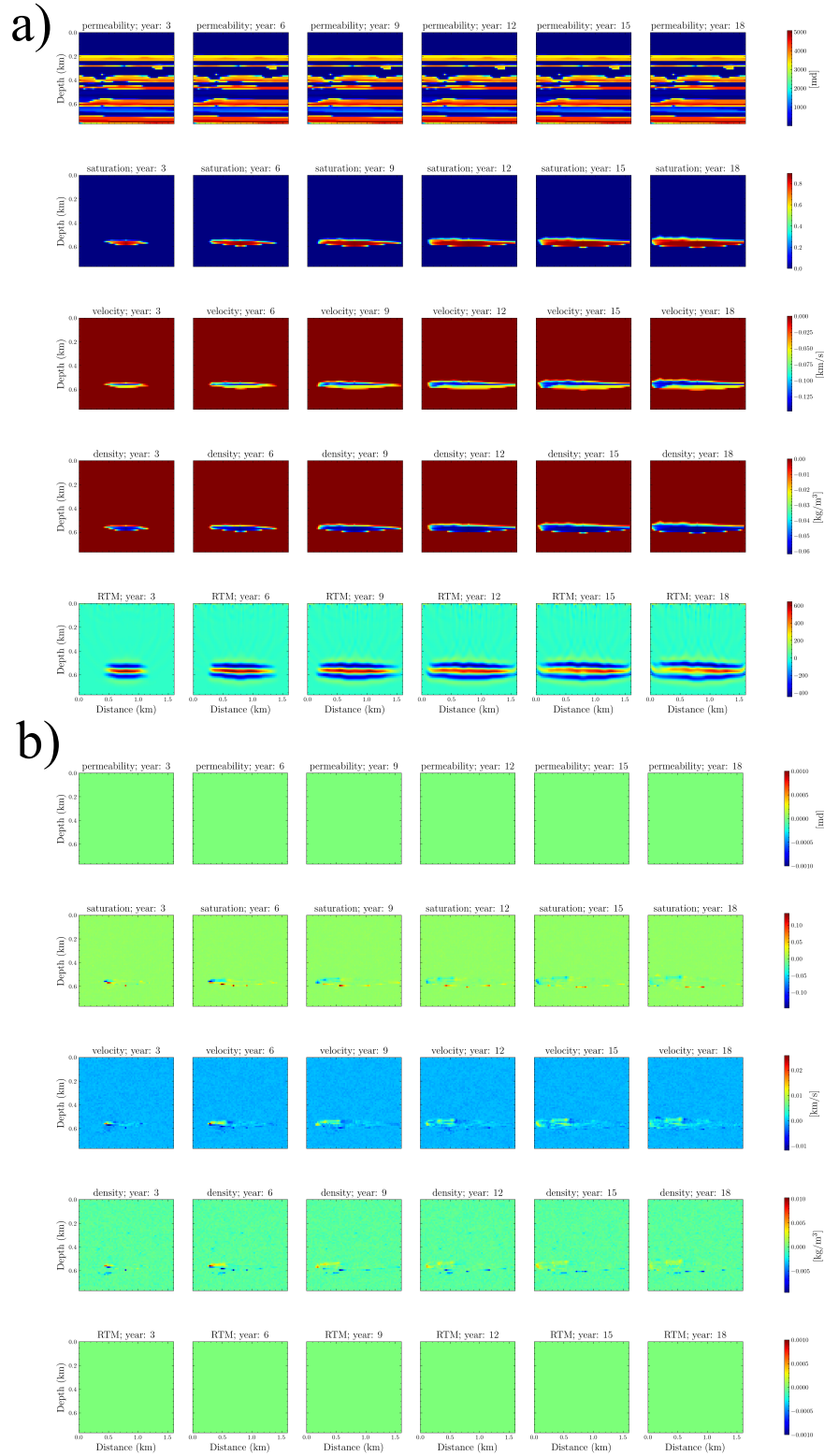


Figure 10: The errors (b) in the inverted results (Figure 9b) compared to the reference result (a). The rows represent the various monitored properties described in Figure 4. The errors (differences) are plotted at the same scale.

permeability (denoted by the red box in Figure 11a) to invert the in-distribution scope (denoted by the blue dashed box in Figure 11a) and, then use the states at 6, 9, 12, 15, and 18 years as history states

to predict the future states at 21 years (denoted by the gray dashed box in Figure 11a) for a proof-of-concept test. In addition, to also test the generalization ability, the injection rate for this sequence is decreased to achieve a 10% storage capacity over a 21-year period. As shown in Figure 11a, the diffusion model captures not only the dynamics over different physical variables but also the dynamics of evolution over time. The predictions over the horizon of training are still reasonable, demonstrating the potential of the proposed method for forecasting beyond the trained horizon. Then, we also simulated the reference results for the comparison. The errors shown in Figure 11b highlight the ability of the proposed framework in the out-of-distribution forecasting task. To improve forecasting accuracy for longer sequences or different injection rates, one can incorporate more time frames during the training while keeping the number of frames for each sample and more sequences using different injection rates.

3.5 Uncertainty analysis

Despite the generally high accuracy we managed to achieve in forecasting and inversion, we still had errors as compared to the numerical simulation the training of the diffusion models was based on. As we saw, the accuracy depends on the amount of data we use to condition the generation. Thus, uncertainty quantification as an additional output of the framework can help us assess confidence in the inversion and forecasting results in practical applications, where reference solutions are unavailable. Recall that our monitoring framework is based on the video diffusion model, which is one type of generative models that naturally supports the uncertainty analysis. The way to quantify approximate uncertainty within our framework is generally simple and cheap. We mainly need perform conditional sampling for the same history states and measurements starting from several random noise samples in parallel, let's say 16 samples for the sake of the test though this number is theoretically small to properly sample the posterior distribution. Thus, we evaluate the mean and standard deviation of the generated 16 evolution samples. We assume a constant permeability in this test and give the three past history states and the RTM image results over the years to perform the inversion. We share one of the samples in Figure 12 as well as the mean prediction in Figure 13. Similar to the performance shown in Sections 3.2 and 3.3, the sample shows highly accurate inversion results, and the consistency of evolution between different variables remains. As for the mean values for those 16 samples, they are close to the reference numerical simulations as expected, but we found that the errors are slightly different compared to the sample shown in Figure 12b. They are larger at the area of the boundary of the CO₂ plume and decrease from the boundary to the interior of the CO₂ plume. This contributes to the uncertainty of the sampling process. The standard deviation values for those 16 samples are shown in Figure 14. As expected, high uncertainty appears at the boundary of the plume, especially around the leakage area, and decreases from the boundary to the interior of the CO₂ plume, consistent with the errors map of the mean predictions. It demonstrates that the proposed method can achieve probabilistic predictions in a fully parallel way and can provide a reasonable approximate uncertainty map.

4 Discussions

This paper presents a novel framework utilizing video diffusion models for subsurface forecasting and monitoring. It demonstrates good performance in terms of physical consistency, visual quality, and accuracy. However, a notable limitation is the computational cost of the sampling process, which necessitates iterative inference (1000 iterations in our case). This issue highlights the need for further optimization to reduce computational cost, possibly through approaches like denoising diffusion implicit models [Song et al., 2022] or consistency models [Song et al., 2023]. In addition, to handle the high-resolution multiphysics images over longer time lapse evolution, where the computational cost is expected to be huge, and the learning complexity increases, advanced techniques such as stable diffusion [Rombach et al., 2022] and [Peebles and Xie, 2022] are needed.

Besides the computational cost, to apply our method in field applications, addressing the gap between the training data and realistic multiphysics evolution is required. Specifically, in realistic scenarios, we may have a time-dependent injection rate rather than a constant one, as used in this paper. In some cases, we might stop the injection for a while and continue later. What's more, the location of the injection well and multiple injection wells should also be considered. Thus, including

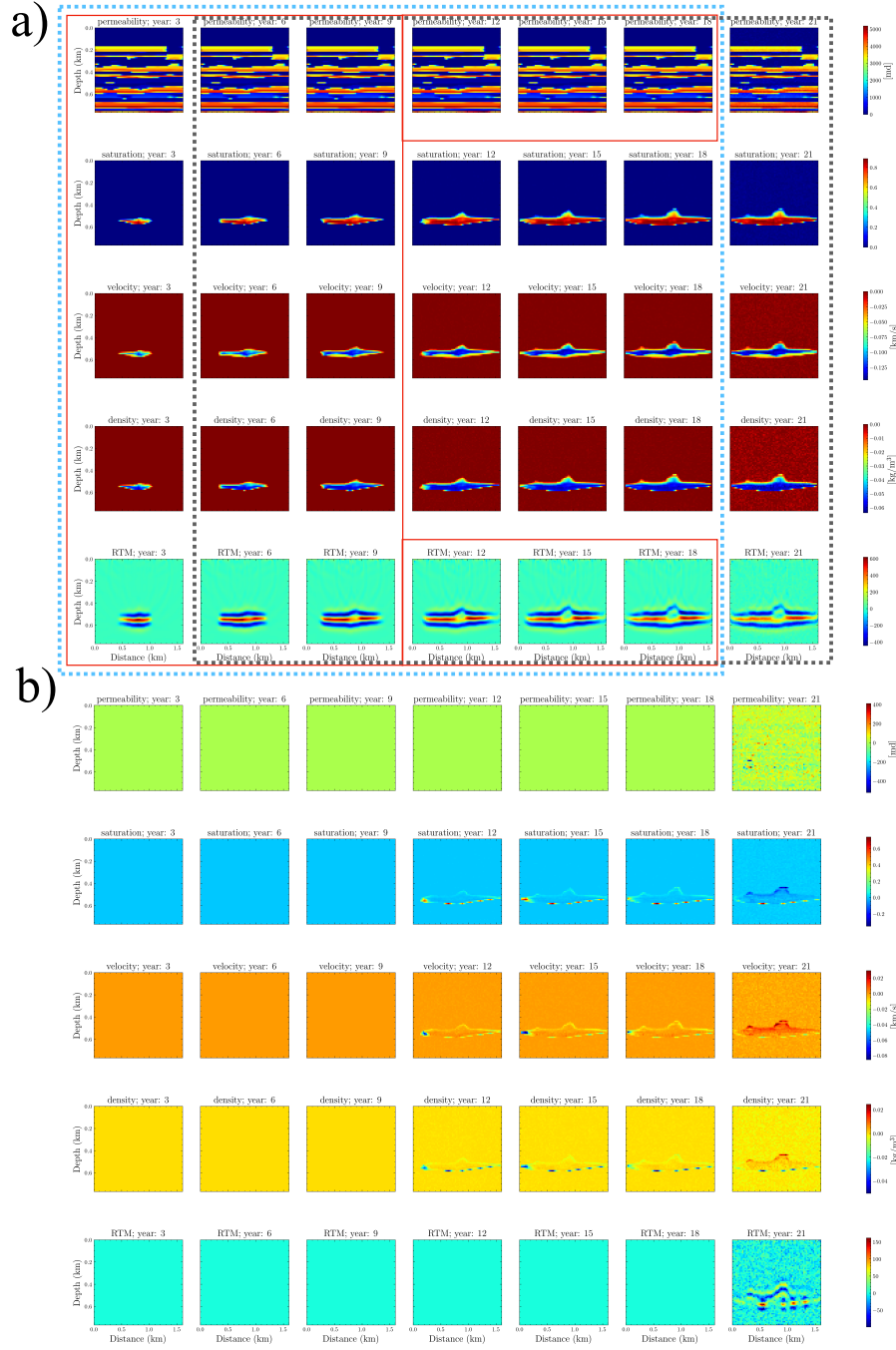


Figure 11: Out-of-horizon autoregressive predictions (a) given three history frames at 3, 6 and 9 years, and permeability and RTM images at 3 to 18 years, which are denoted by the red box. The first prediction is denoted by the blue dashed box while the second autoregressive prediction is highlighted by the gray dashed box. (b) shows the errors between the forecasting results and numerical simulated ones.

such a variable would be more interesting and important. The classifier-free conditional diffusion model [Ho and Salimans, 2021, Wang et al., 2024] would be a potential solution, which we might explore more in the future. For example, we can have the injection rate over a period as a condition, as such information is often known.

In the current pipeline, we use RTM images as the seismic response rather than the seismic recordings. The adaption to seismic recordings also requires video diffusion models to learn a mapping from

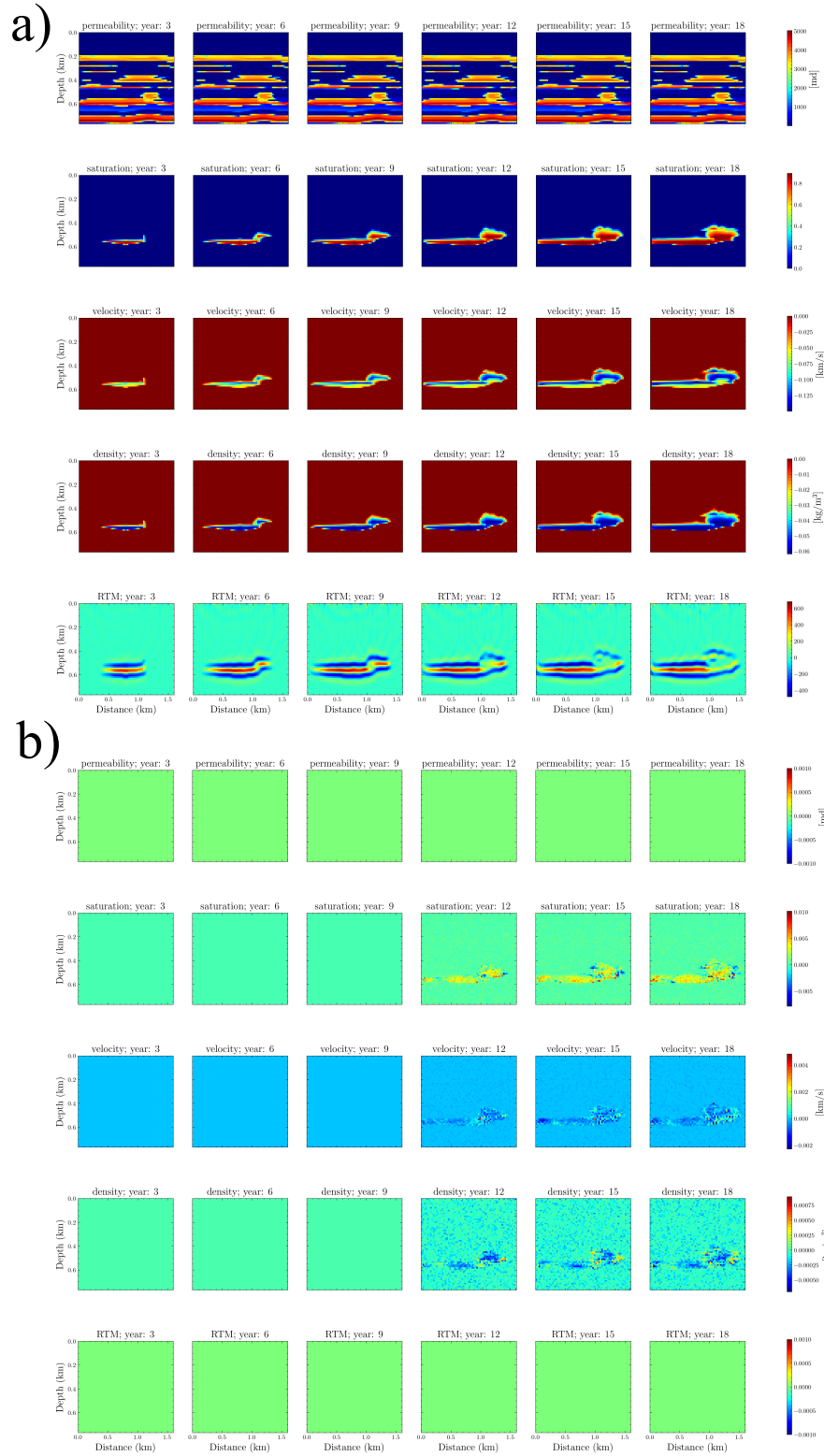


Figure 12: A sample (a) from the 16 inverted results given three history frames, constant permeability, and observed RTM images. (b) shows the errors between (a) and the reference numerical simulations.

the velocity and density to the seismic waveform. This mapping, as we know from full waveform inversion, is very complicated, requiring an abundance of training data, and often lacks generalization abilities. Although the ideal workflow is to enable the inversion or forecasting based on the observed

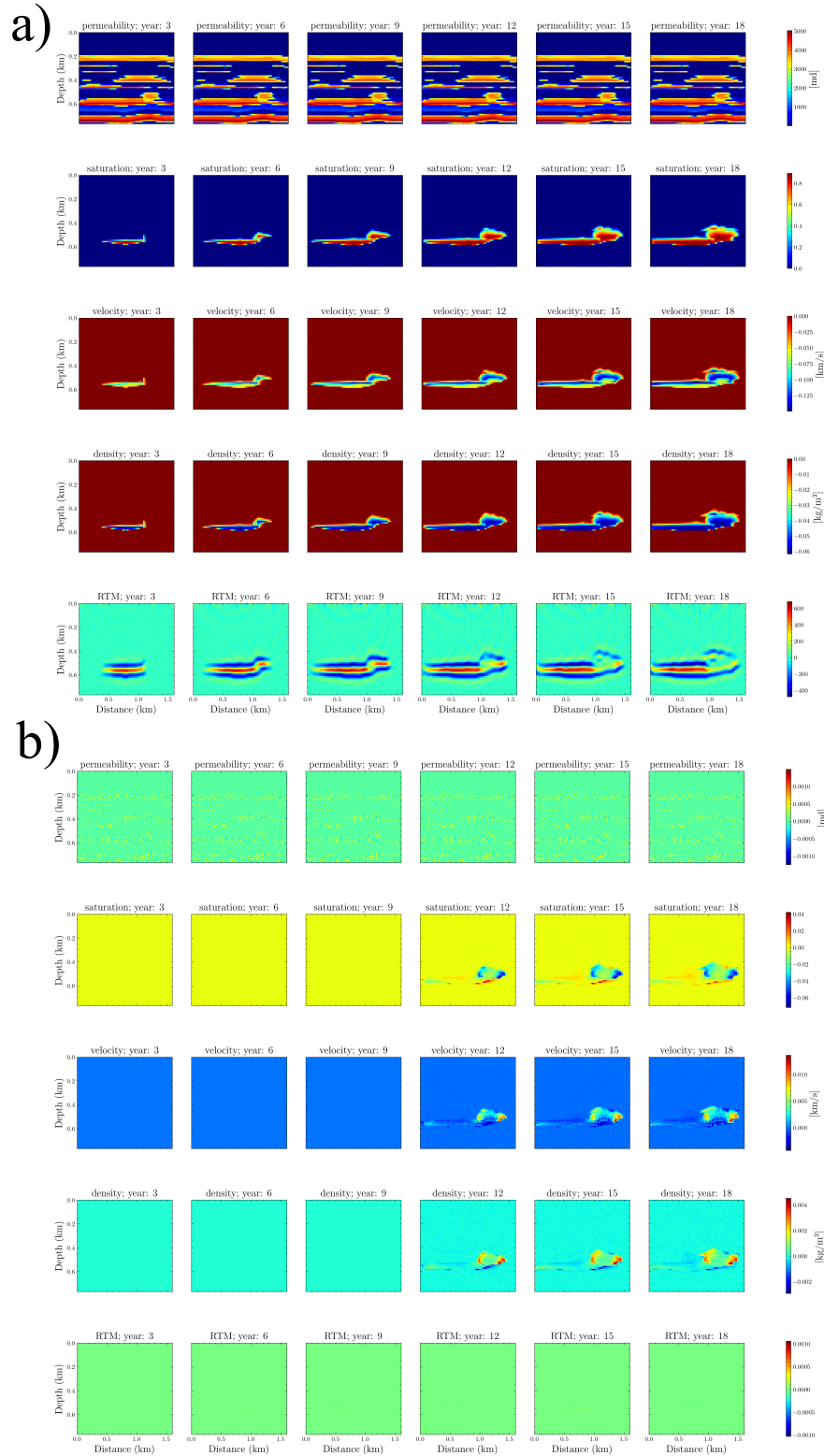


Figure 13: The mean prediction of 16 inverted results (a) given three history frames, constant permeability, and observed RTM images starting from different random noises. (b) shows the errors between (a) and the reference numerical simulations.

seismic data, which is quite straightforward in realistic monitoring scenarios, such an undertaking will increase the complexity of the whole multiphysics process further as we need to teach the neural

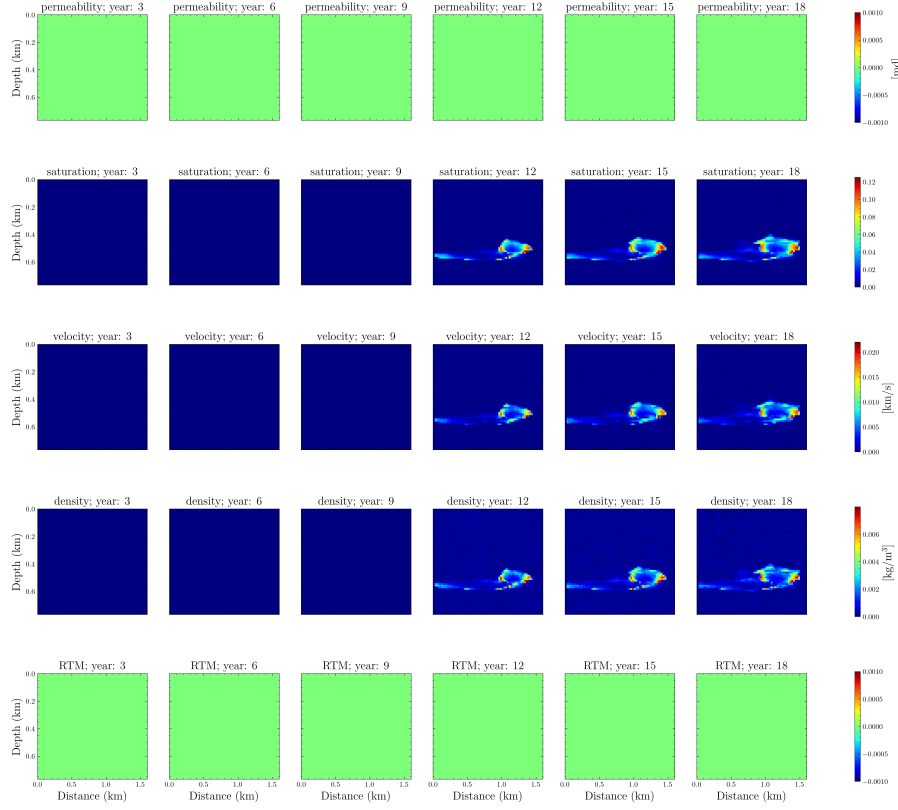


Figure 14: The standard deviation of 16 inverted results given three history frames, constant permeability, and observed RTM images starting from different random noises.

network to learn the wave-equation modeling engine. This challenge reveals another interesting future direction, in which we can try to learn a neural PDE solver [Huang et al., 2024, Huang and Alkhalifah, 2024b] for instant seismic modeling given the velocity and geometry or directly incorporate the differential seismic wavefield modeling engine, such as DeepWave [Richardson, 2023], into the monitoring framework.

Unlike neural PDE solvers, which can learn simulation mappings between the given input multiple variables and the corresponding CO₂ saturations, velocity, and so on, the proposed framework directly learns the end-to-end multiphysics evolution by processing them as video. Since the physical world and complex physical phenomena like CO₂ multiphysics evolution can be hypothetically filmed and captured as a video, using a video diffusion model to store such evolution, including the physics involved, seems natural. Beyond the demonstration in this paper for this concept, there are also many literatures showing that the video diffusion models can simulate the world [Cachay et al., 2023, Price et al., 2023, Ding et al., 2024]. However, to make the diffusion models store the real physics and generate the evolution with arbitrary length, a large amount of training samples are needed. In addition, as shown in the paper, the forecasting results still exhibit errors compared to the reference results. To further enhance the performance and reduce the number of training samples, we believe that incorporating the physical knowledge, for example, the governing equations as a physics-constraint loss [Huang and Alkhalifah, 2022, 2024a, Huang et al., 2024, Christopher et al., 2024], in the sampling process can enhance the dynamic consistency over time, and correct the errors. To improve the forecasting ability to longer future horizons, combining the next-token prediction models, which enable variable-length generation, with the video diffusion models, e.g., diffusion forcing [Chen et al., 2024], might be a potential solution path for framework.

5 Conclusions

We proposed a novel subsurface multiphysics monitoring and forecasting framework utilizing video diffusion models. Our method demonstrates the ability to generate high-quality representations of CO₂ evolution and associated changes in subsurface elastic properties. With reconstruction guidance, it shows promising results in forecasting and inversion based on historical frames and observational data. Additionally, thanks to the diffusion model’s inherent support for uncertainty quantification, our framework provides an efficient way for conducting reasonable uncertainty quantification. The test on the Compass model demonstrates the effectiveness of the proposed method and the potential of the proposed method as the unified framework for forecasting, inversion, and uncertainty analysis of CO₂ related multiphysics monitoring and inversion.

6 Acknowledgements

We thank KAUST and the sponsors of the Deepwave Consortium for their support. We also thank Ziyi Yin for the discussion on data generation. This work utilized the resources of the Supercomputing Laboratory at KAUST, and we are grateful for that.

References

- M. Bosch, T. Mukerji, and E. F. Gonzalez. Seismic inversion for reservoir properties combining statistical rock physics and geostatistics: A review. *GEOPHYSICS*, 75(5):75A165–75A176, Sept. 2010. ISSN 0016-8033. doi: 10.1190/1.3478209. URL <https://library.seg.org/doi/10.1190/1.3478209>. Publisher: Society of Exploration Geophysicists.
- S. R. Cachay, B. Zhao, H. Joren, and R. Yu. DYffusion: A Dynamics-informed Diffusion Model for Spatiotemporal Forecasting, Oct. 2023. URL <http://arxiv.org/abs/2306.01984>. arXiv:2306.01984 [cs, stat].
- B. Chen, D. M. Monso, Y. Du, M. Simchowitz, R. Tedrake, and V. Sitzmann. Diffusion Forcing: Next-token Prediction Meets Full-Sequence Diffusion, July 2024. URL <http://arxiv.org/abs/2407.01392>. arXiv:2407.01392 [cs].
- J. K. Christopher, S. Baek, and F. Fioretto. Projected Generative Diffusion Models for Constraint Satisfaction, Feb. 2024. URL <http://arxiv.org/abs/2402.03559>. arXiv:2402.03559 [cs].
- O. Cicek, A. Abdulkadir, S. S. Lienkamp, T. Brox, and O. Ronneberger. 3D U-Net: Learning Dense Volumetric Segmentation from Sparse Annotation, June 2016. URL <http://arxiv.org/abs/1606.06650>. arXiv:1606.06650 [cs].
- Z. Ding, A. Zhang, Y. Tian, and Q. Zheng. Diffusion World Model, Feb. 2024. URL <http://arxiv.org/abs/2402.03570>. arXiv:2402.03570 [cs].
- S. Fort, H. Hu, and B. Lakshminarayanan. Deep Ensembles: A Loss Landscape Perspective, June 2020. URL <http://arxiv.org/abs/1912.02757>. arXiv:1912.02757 [cs, stat].
- A. P. Gahlot, H. T. Erdinc, R. Orozco, Z. Yin, and F. J. Herrmann. Inference of CO₂ flow patterns – a feasibility study, Nov. 2023. URL <http://arxiv.org/abs/2311.00290>. arXiv:2311.00290 [math-ph, physics:physics].
- I. Goodfellow, J. Pouget-Abadie, M. Mirza, B. Xu, D. Warde-Farley, S. Ozair, A. Courville, and Y. Bengio. Generative Adversarial Nets. In *Advances in Neural Information Processing Systems*, volume 27. Curran Associates, Inc., 2014. URL https://proceedings.neurips.cc/paper_files/paper/2014/hash/5ca3e9b122f61f8f06494c97b1afccf3-Abstract.html.
- E. Hicks, H. Hoeber, M. Houbiers, S. P. Lescoffit, A. Ratcliffe, and V. Vinje. Time-lapse full-waveform inversion as a reservoir-monitoring tool — A North Sea case study. *The Leading Edge*, 35(10):850–858, Oct. 2016. ISSN 1070-485X. doi: 10.1190/tle35100850.1. URL <https://library.seg.org/doi/abs/10.1190/tle35100850.1>. Publisher: Society of Exploration Geophysicists.

- J. Ho and T. Salimans. Classifier-Free Diffusion Guidance. *NeurIPS 2021 Workshop on Deep Generative Models and Downstream Applications*, 2021.
- J. Ho, A. Jain, and P. Abbeel. Denoising Diffusion Probabilistic Models. In *34th Conference on Neural Information Processing Systems*, page 25, 2020.
- J. Ho, T. Salimans, A. Gritsenko, W. Chan, M. Norouzi, and D. J. Fleet. Video Diffusion Models, June 2022. URL <http://arxiv.org/abs/2204.03458>. arXiv:2204.03458 [cs].
- Q. Hu, D. Grana, and K. A. Innanen. Feasibility of seismic time-lapse monitoring of CO₂ with rock physics parametrized full waveform inversion. *Geophysical Journal International*, 233(1):402–419, Apr. 2023. ISSN 0956-540X. doi: 10.1093/gji/ggac462. URL <https://doi.org/10.1093/gji/ggac462>.
- X. Huang and T. Alkhalifah. PINNup: Robust Neural Network Wavefield Solutions Using Frequency Upscaling and Neuron Splitting. *Journal of Geophysical Research: Solid Earth*, 127(6):e2021JB023703, 2022. ISSN 2169-9356. doi: 10.1029/2021JB023703. URL <https://onlinelibrary.wiley.com/doi/abs/10.1029/2021JB023703>. _eprint: <https://onlinelibrary.wiley.com/doi/pdf/10.1029/2021JB023703>.
- X. Huang and T. Alkhalifah. Efficient physics-informed neural networks using hash encoding. *Journal of Computational Physics*, 501:112760, Mar. 2024a. ISSN 0021-9991. doi: 10.1016/j.jcp.2024.112760. URL <https://www.sciencedirect.com/science/article/pii/S0021999124000093>.
- X. Huang and T. Alkhalifah. Learned frequency-domain scattered wavefield solutions using neural operators, May 2024b. URL <http://arxiv.org/abs/2405.01272>. arXiv:2405.01272 [physics].
- X. Huang, W. Shi, X. Gao, X. Wei, J. Zhang, J. Bian, M. Yang, and T.-Y. Liu. LordNet: An efficient neural network for learning to solve parametric partial differential equations without simulated data. *Neural Networks*, 176:106354, Aug. 2024. ISSN 0893-6080. doi: 10.1016/j.neunet.2024.106354. URL <https://www.sciencedirect.com/science/article/pii/S0893608024002788>.
- IPCC. *Climate Change 2022: Mitigation of Climate Change. Contribution of Working Group III to the Sixth Assessment Report of the Intergovernmental Panel on Climate Change*. Cambridge University Press., 2022.
- C. E. Jones, J. A. Edgar, J. I. Selvage, and H. Crook. Building Complex Synthetic Models to Evaluate Acquisition Geometries and Velocity Inversion Technologies. In *74th EAGE Annual Conference & Exhibition*, page cp. European Association of Geoscientists & Engineers, June 2012. ISBN 978-90-73834-27-9. doi: 10.3997/2214-4609.20148575. URL <https://www.earthdoc.org/content/papers/10.3997/2214-4609.20148575>. ISSN: 2214-4609.
- D. P. Kingma and M. Welling. Auto-Encoding Variational Bayes, 2013. URL <http://arxiv.org/abs/1312.6114>. arXiv:1312.6114 [cs, stat].
- B. Li and Y. E. Li. Neural Network-Based CO₂ Interpretation From 4D Sleipner Seismic Images. *Journal of Geophysical Research: Solid Earth*, 126(12):e2021JB022524, 2021. ISSN 2169-9356. doi: 10.1029/2021JB022524. URL <https://onlinelibrary.wiley.com/doi/abs/10.1029/2021JB022524>. _eprint: <https://onlinelibrary.wiley.com/doi/pdf/10.1029/2021JB022524>.
- B. Li, F. Zhou, H. Li, A. Duguid, L. Que, Y. Xue, and Y. Tan. Prediction of CO₂ leakage risk for wells in carbon sequestration fields with an optimal artificial neural network. *International Journal of Greenhouse Gas Control*, 68:276–286, Jan. 2018. ISSN 1750-5836. doi: 10.1016/j.ijggc.2017.11.004. URL <https://www.sciencedirect.com/science/article/pii/S1750583617303237>.
- D. Li, K. Xu, J. M. Harris, and E. Darve. Coupled Time-Lapse Full-Waveform Inversion for Subsurface Flow Problems Using Intrusive Automatic Differentiation. *Water Resources Research*, 56(8):e2019WR027032, 2020. ISSN 1944-7973. doi: 10.1029/2019WR027032. URL <https://onlinelibrary.wiley.com/doi/abs/10.1029/2019WR027032>. _eprint: <https://onlinelibrary.wiley.com/doi/pdf/10.1029/2019WR027032>.

- Y. Li and T. Alkhalifah. Target-Oriented Time-Lapse Elastic Full-Waveform Inversion Constrained by Deep Learning-Based Prior Model. *IEEE Transactions on Geoscience and Remote Sensing*, 60:1–12, 2022. ISSN 0196-2892, 1558-0644. doi: 10.1109/TGRS.2022.3186028. URL <https://ieeexplore.ieee.org/document/9808328/>.
- M. Louboutin, P. Witte, Z. Yin, H. Modzelewski, Kerim, C. d. Costa, and P. Nogueira. slim-group/JUDI.jl: v3.2.3, Mar. 2023a. URL <https://zenodo.org/records/7785440>.
- M. Louboutin, Z. Yin, R. Orozco, T. J. Grady, A. Siahkoohi, G. Rizzuti, P. A. Witte, O. Møyner, G. J. Gorman, and F. J. Herrmann. Learned multiphysics inversion with differentiable programming and machine learning. *The Leading Edge*, 42(7):474–486, July 2023b. ISSN 1070-485X, 1938-3789. doi: 10.1190/tle42070474.1. URL <https://library.seg.org/doi/10.1190/tle42070474.1>.
- D. Lumley. 4D seismic monitoring of CO₂ sequestration. *The Leading Edge*, 29(2):150–155, Feb. 2010. ISSN 1070-485X, 1938-3789. doi: 10.1190/1.3304817. URL <https://library.seg.org/doi/10.1190/1.3304817>.
- P. Micikevicius, S. Narang, J. Alben, G. Diamos, E. Elsen, D. Garcia, B. Ginsburg, M. Houston, O. Kuchaiev, G. Venkatesh, and H. Wu. Mixed Precision Training, Feb. 2018. URL <http://arxiv.org/abs/1710.03740>. arXiv:1710.03740 [cs, stat].
- O. Møyner, M. Johnsrud, H. M. Nilsen, X. Raynaud, K. O. Lye, and Z. Yin. sintefmath/Jutul.jl: v0.2.6, Apr. 2023. URL <https://zenodo.org/records/7855605>.
- A. Q. Nichol and P. Dhariwal. Improved Denoising Diffusion Probabilistic Models. In *Proceedings of the 38th International Conference on Machine Learning*, pages 8162–8171. PMLR, July 2021. URL <https://proceedings.mlr.press/v139/nichol21a.html>. ISSN: 2640-3498.
- W. Peebles and S. Xie. Scalable Diffusion Models with Transformers, Dec. 2022. URL <http://arxiv.org/abs/2212.09748>. arXiv:2212.09748 [cs].
- I. Price, A. Sanchez-Gonzalez, F. Alet, T. Ewalds, A. El-Kadi, J. Stott, S. Mohamed, P. Battaglia, R. Lam, and M. Willson. GenCast: Diffusion-based ensemble forecasting for medium-range weather, Dec. 2023. URL <http://arxiv.org/abs/2312.15796>. arXiv:2312.15796 [physics].
- K. Pruess and J. Nordbotten. Numerical Simulation Studies of the Long-term Evolution of a CO₂ Plume in a Saline Aquifer with a Sloping Caprock. *Transport in Porous Media*, 90(1):135–151, Oct. 2011. ISSN 0169-3913, 1573-1634. doi: 10.1007/s11242-011-9729-6. URL <http://link.springer.com/10.1007/s11242-011-9729-6>.
- D. Rezende and S. Mohamed. Variational Inference with Normalizing Flows. In *Proceedings of the 32nd International Conference on Machine Learning*, pages 1530–1538. PMLR, June 2015. URL <https://proceedings.mlr.press/v37/rezende15.html>. ISSN: 1938-7228.
- A. Richardson. Deepwave, Sept. 2023. URL <https://zenodo.org/records/8381177>.
- R. Rombach, A. Blattmann, D. Lorenz, P. Esser, and B. Ommer. High-Resolution Image Synthesis with Latent Diffusion Models, Apr. 2022. URL <http://arxiv.org/abs/2112.10752>. arXiv:2112.10752 [cs].
- P. Shaw, J. Uszkoreit, and A. Vaswani. Self-Attention with Relative Position Representations, Apr. 2018. URL <http://arxiv.org/abs/1803.02155>. arXiv:1803.02155 [cs].
- J. Song, C. Meng, and S. Ermon. Denoising Diffusion Implicit Models, Oct. 2022. URL <http://arxiv.org/abs/2010.02502>. arXiv:2010.02502 [cs].
- Y. Song, P. Dhariwal, M. Chen, and I. Sutskever. Consistency Models, Mar. 2023. URL <http://arxiv.org/abs/2303.01469>. arXiv:2303.01469 [cs, stat].
- M. Stepien, C. A. Ferreira, S. Hosseinzadehsadati, T. Kadeethum, and H. M. Nick. Continuous conditional generative adversarial networks for data-driven modelling of geologic CO₂ storage and plume evolution. *Gas Science and Engineering*, 115:204982, July 2023. ISSN 29499089. doi: 10.1016/j.jgsce.2023.204982. URL <https://linkinghub.elsevier.com/retrieve/pii/S2949908923001103>.

- A. Y. Sun, Z. X. Leong, and T. Zhu. A denoising diffusion probabilistic modeling approach for predicting CO₂ plume evolution from seismic shot gathers. In *Third International Meeting for Applied Geoscience & Energy Expanded Abstracts*, pages 376–380, Houston, Texas, Dec. 2023. Society of Exploration Geophysicists and American Association of Petroleum Geologists. doi: 10.1190/image2023-3915826.1. URL <https://library.seg.org/doi/10.1190/image2023-3915826.1>.
- F. Wang, X. Huang, and T. Alkhalifah. Controllable seismic velocity synthesis using generative diffusion models, Feb. 2024. URL <http://arxiv.org/abs/2402.06277>. arXiv:2402.06277 [physics].
- G. Wen, C. Hay, and S. M. Benson. CCSNet: A deep learning modeling suite for CO₂ storage. *Advances in Water Resources*, 155:104009, Sept. 2021. ISSN 03091708. doi: 10.1016/j.advwatres.2021.104009. URL <https://linkinghub.elsevier.com/retrieve/pii/S0309170821001640>.
- G. Wen, Z. Li, Q. Long, K. Azizzadenesheli, A. Anandkumar, and S. M. Benson. Accelerating Carbon Capture and Storage Modeling using Fourier Neural Operators, Oct. 2022. URL <http://arxiv.org/abs/2210.17051>. arXiv:2210.17051 [physics].
- A. G. Wilson and P. Izmailov. Bayesian Deep Learning and a Probabilistic Perspective of Generalization, Mar. 2022. URL <http://arxiv.org/abs/2002.08791>. arXiv:2002.08791 [cs, stat].
- P. A. Witte, T. Konuk, E. Skjetne, and R. Chandra. Fast CO₂ saturation simulations on large-scale geomodels with artificial intelligence-based Wavelet Neural Operators. *International Journal of Greenhouse Gas Control*, 126:103880, June 2023. ISSN 17505836. doi: 10.1016/j.ijggc.2023.103880. URL <https://linkinghub.elsevier.com/retrieve/pii/S1750583623000506>.
- T. Xu, P. Mi, R. Wang, and Y. Chen. Towards Faster Training of Diffusion Models: An Inspiration of A Consistency Phenomenon, Mar. 2024. URL <http://arxiv.org/abs/2404.07946>. arXiv:2404.07946 [cs].
- Z. Yin. slimgroup/Seis4CCS.jl, 2022. URL <https://github.com/slimgroup/Seis4CCS.jl>. original-date: 2021-06-02T16:32:38Z.
- Z. Yin, G. Bruer, and M. Louboutin. slimgroup/JutulDarcyRules.jl: v0.2.5, Apr. 2023a. URL <https://zenodo.org/records/7863970>.
- Z. Yin, H. T. Erdinc, A. P. Gahlot, M. Louboutin, and F. J. Herrmann. Derisking geologic carbon storage from high-resolution time-lapse seismic to explainable leakage detection. *The Leading Edge*, 42(1):69–76, Jan. 2023b. ISSN 1070-485X. doi: 10.1190/tle42010069.1. URL <https://library.seg.org/doi/full/10.1190/tle42010069.1>. Publisher: Society of Exploration Geophysicists.
- Z. Zhong, A. Y. Sun, and H. Jeong. Predicting CO₂ Plume Migration in Heterogeneous Formations Using Conditional Deep Convolutional Generative Adversarial Network. *Water Resources Research*, 55(7):5830–5851, 2019. ISSN 1944-7973. doi: 10.1029/2018WR024592. URL <https://onlinelibrary.wiley.com/doi/abs/10.1029/2018WR024592>. eprint: <https://onlinelibrary.wiley.com/doi/pdf/10.1029/2018WR024592>.
- Z. Zhou, Y. Lin, Z. Zhang, Y. Wu, Z. Wang, R. Dilmore, and G. Guthrie. A data-driven CO₂ leakage detection using seismic data and spatial-temporal densely connected convolutional neural networks. *International Journal of Greenhouse Gas Control*, 90:102790, Nov. 2019. ISSN 1750-5836. doi: 10.1016/j.ijggc.2019.102790. URL <https://www.sciencedirect.com/science/article/pii/S1750583619301239>.